Trajectory engineering of directrons in liquid crystals via photoalignment

DOI:
10.1039/D3SM00377A

Document Version
Final published version

Soft Matter

PAPER

View Article Online
View Journal

Cite this: DOI: 10.1039/d3sm00377a

Trajectory engineering of directrons in liquid crystals *via* photoalignment†

Ke-Hui Wu,[a] Chang-Qi Chen,[a] Yuan Shen,[b] Yu Cao,[a] Sen-Sen Li,*[ac] Ingo Dierking[b] and Lu-Jian Chen*[ac]

Received 22nd March 2023,
Accepted 23rd May 2023

DOI: 10.1039/d3sm00377a

rsc.li/soft-matter-journal

As electrically generated solitons in liquid crystals, directrons represent intriguing structures promising extensive application prospects in the areas of microcargo vehicles, microreactors, and logic devices. However, manipulating directrons along elaborate predetermined trajectories still remains to be largely explored. In this work, the strategy of constructing high-resolution periodic alignment fields for directrons *via* the polarization holography photoalignment technique is presented. The optimum exposure dose for directrons to form over a broad range of electric fields is determined to be 32.4 J cm^{-2} for the alignment layers with 1 wt% azo dye SD1. Zigzag and fishhook-shaped trajectories of directrons are realized with two orthogonal polarized beams. The resolution for zigzag steering of directrons is evaluated to be approximately 56 μm to 80 μm, about three to four times the length of directrons. These results not only enrich the forms of motion of directrons, but also lay the foundations for customized trajectories of directrons in future developments.

Introduction

Solitons are synonymous with localized waves in the general physics literature.[1] They are ubiquitous and exist in various systems from the sky to the laboratory, such as Jupiter's great red spot,[2,3] vortex lines in Bose–Einstein condensates[4] and magnetic materials,[5] just to name a few. Nevertheless, the artificial generation and manipulation of multi-dimensional solitons are still facing substantial challenges. Fortunately, liquid crystals (LCs), as a typical type of soft functional matter, provide an excellent material platform for experimental studies of solitons due to their manifold effective means of control. Investigations on solitons in LCs have a history of over 50 years since the first discussion carried out in 1968.[1,6] There are three distinct varieties of soliton objects met in LCs, topological solitons,[7–9] nematicons,[10–13] and directrons.[14–17] Remarkably, directrons refer to dissipative solitons taking the form of particle-like solitary waves of the directors in electrically driven nematics. Originally, dynamic butterfly-shaped director deformations in the electroconvection of nematics were observed by Brand *et al.* in 1997,[18] which could not be predicted by the hydrodynamic model, and did not receive much attention. Only recently, Li *et al.* revealed that similar formations are three-dimensional solitary waves of director deformations driven by a uniform electric field,[14,15] and coined the term 'directrons'.[19] Since then, a number of directrons exhibiting intriguing dynamic behaviors have been generated and reported in both achiral and chiral nematics.[14–17,20–23]

Directrons represent self-confined localized director oscillations that can propagate for a distance of at least the order of centimetres, limited by the cell size. As autonomous structures in electrically driven LCs, a wide range of novel and diverse applications for directrons have been proposed, including microcargo vehicles,[15,19,24] microreactors in chemical systems,[22] and logic devices for signal transduction[25] and even computation.[25] Among them, the targeted delivery capability of directrons has been demonstrated. An impurity surrounded by a directron was transported over a distance of one hundred times its size in just a few seconds.[20] This directron-induced LC-enabled electrophoresis was also utilized to transport microscopic cargoes such as polystyrene spheres.[24] Trajectory manipulation is of fundamental importance to adapt directrons for all of the possible applications. For this it is of benefit that one of the striking features of directrons is that their trajectories can be controlled not only by electric fields, but also by the alignment layers.

So far the initial alignments for directrons have been obtained using mechanical rubbing,[14–16] the photoalignment technique,[17,20] or surface chemistry.[22] With uniform rubbing alignment, at first directrons simply traveled in straight lines,

[a] Department of Electronic Engineering, School of Electronic Science and Engineering, Xiamen University, Xiamen 361005, China. E-mail: sensenli@xmu.edu.cn, lujianchen@xmu.edu.cn
[b] Department of Physics and Astronomy, School of Natural Sciences, University of Manchester, Oxford Road, Manchester M13 9PL, UK
[c] Fujian Key Laboratory of Ultrafast Laser Technology and Applications, Xiamen University, Xiamen, China

† Electronic supplementary information (ESI) available. See DOI: https://doi.org/10.1039/d3sm00377a

then their motion were steered around 90 degree by the step-like amplitude change of driving electric field,[15] and almost at the same time the fractalised proliferation trajectory of destabilised directrons was reported.[16] Shortly afterwards, the propagation direction of directrons was consecutively deflected twice by 45 degrees[20] or turned directly by 90 degrees[17] while maintaining the alternating current (AC) electric field unchanged. This was achieved through the photoalignment technique with two or three regions of different alignment directions.[17,20] Additionally, a range of directron behaviors including refraction, reflection, and splitting were discovered, at the boundary between two LC domains with uniform and twisted director alignments induced by surface chemistry.[22] However, the feasibility of designing more exquisite alignment layers to realize more complicated directron trajectories remains to be explored. The photoalignment technique is an excellent candidate for intricate alignment arrangements since it is suitable to high-resolution multidomain alignments.[26] Moreover, photoalignment can avoid mechanical damage, electrostatic charge, and dust contamination present through the conventional rubbing technique. Although the photoalignment technique has been introduced to convert the directron trajectory as mentioned earlier, there are still many unknown aspects needed to be studied further, such as the optimum exposure dose for directron generation, and the highest possible resolution of trajectory engineering.

In this work, we demonstrate the generation and structure of directrons with homogeneous photoalignment by linearly polarized light, which exhibit many features similar to those reported for PI (polyimide) treated surfaces. The exposure dose for the alignment process is optimized by analyzing the phase diagrams of four states of director orientations including directrons. Based on these results, the polarization holography alignment technique with two orthogonal polarized beams is employed, to construct elaborate alignment layers with high-resolution periodic alignments to steer directrons along zigzag and fishhook-shaped trajectories. Furthermore, the resolution for zigzag manipulation of directrons is evaluated, and compared with the spatial dimension of directrons.

Result and discussion

Materials and experimental design

A commercially available nematic LC 4′-butyl-4-heptyl-bicyclohexyl-4-carbonitrile (CCN-47) with negative dielectric and conductive anisotropies was used as the LC medium for directron generation. A small amount of 0.005 wt% Tetrabutylammonium bromide (TBAB) was mixed with CCN-47 to tune its net conductivity. The photoalignment technology was employed as a promising approach to generate multidomain LC orientations for exploring multifarious directron trajectories. A polarization-sensitive sulfonic azo dye SD1 was utilized as the photoalignment agent, the chemical structure and absorption spectra of which are shown in Fig. S1 (ESI†). The SD1 molecules tend to cause nematic films of CCN-47 to adopt a planar orientation with an azimuthal direction perpendicular to the UV light polarization due to the *cis-trans* isomerization process.[27] SD1 dissolved in dimethylformamide (DMF) at a concentration of 1 wt% were coated onto the indium tin oxide (ITO) electrodes of the LC cell substrates *via* spin coating. Subsequently, the empty LC cells were photo-aligned homogeneously by linearly polarized light of wavelength λ = 405 nm, and filled with the mixture of CCN-47 and TBAB, to examine the optimum exposure dose for directron

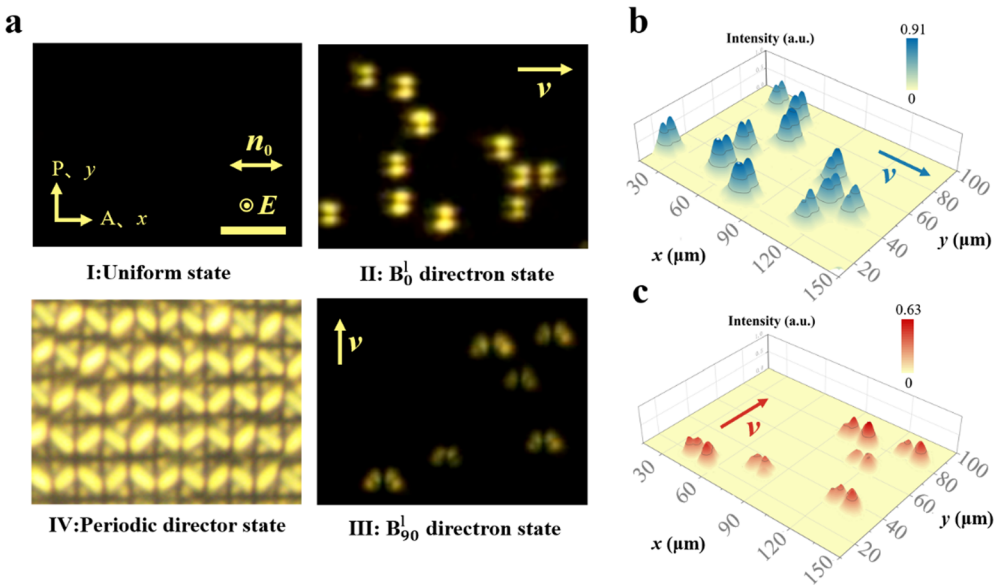

Fig. 1 Four states of director orientations that include directrons. (a) Crossed POM images of I uniform state, II B_0^l directron state, III B_{90}^l directron state, and IV periodic director state. $\boldsymbol{n}_0$ denotes the alignment direction, $\boldsymbol{E}$ indicates the electric field perpendicular to the *xy* plane, and $\boldsymbol{v}$ represents the velocity of the directrons. A and P signify the analyzer and polarizer parallel to the *x* and *y* axis, respectively. The scale bar is 50 μm. Light intensity distributions of (b) II B_0^l directron state and (c) III B_{90}^l directron state.

generation. The rest of empty LC cells were further photo-aligned with a certain periodicity employing the polarization holography alignment technique based on the optimum exposure dose, and filled with the mixture sample, to explore more complicated directron trajectories, and to evaluate the resolution of directron trajectory engineering.

Generation and structure of directrons with photoalignment

The sandwich cells composed of two glass substrates coated with ITO electrode and SD1 photoalignment layer were photo-aligned along the x axis (Fig. 1a), resulting in an alignment direction $\boldsymbol{n}_0$ = (1,0,0). Directrons require an applied electric field to maintain their localized structures and will vanish if the field is removed. An AC electric field $\boldsymbol{E}$ = (0,0,E) at low frequency (f < 100 Hz) was applied to the nematic sample perpendicular to the xy plane (Fig. 1a). Polarizing optical microscopy (POM) observation with crossed polarizers indicates that depending on electric field frequency and amplitude the nematic sample appears in four different states of director configuration (Fig. 1a) that include directrons. Similar to prior reports of directron formation between PI-2555 alignment layers with uniform mechanical rubbing, directrons labeled as B_0^l or B_{90}^l[15,19] (II, III in Fig. 1a) were observed at the edges of the electrodes or as low contrast defects for small frequencies, 5 Hz $\leq f \leq$ 30 Hz, and low amplitudes, 0.5 V μm^{-1} $\leq E \leq$ 1.91 V μm^{-1}. The superscript l thus indicates low frequency (f < 100 Hz) and the subscripts 0 and 90 represent the angle between directron velocity $\boldsymbol{v}$ and the alignment direction $\boldsymbol{n}_0$. The directron states are localized director deformations travelling parallel or perpendicular to $\boldsymbol{n}_0$. Besides the two directron states, the nematic sample exhibits the uniform state and the periodic director state (I, IV in Fig. 1a) for smaller and larger $\boldsymbol{E}$, respectively. The uniform state is observed when $\boldsymbol{n}_0$ is parallel to the polarizer or analyzer direction. The periodic director state is initially generated at the edges of the electrodes and eventually covers the entire cell in seconds. The light intensity distributions of the B_0^l and B_{90}^l states, defined as the gray-scale value distributions of directrons divided by 255, are presented in Fig. 1b, c and Fig. S2 (ESI†), respectively. The higher light intensity of B_0^l directrons may indicate the larger azimuthal deviations of directors from the initial alignment. The structure differences between B_0^l and B_{90}^l directrons obtained by photoalignment are similar to those observed for rubbing alignment when concerning

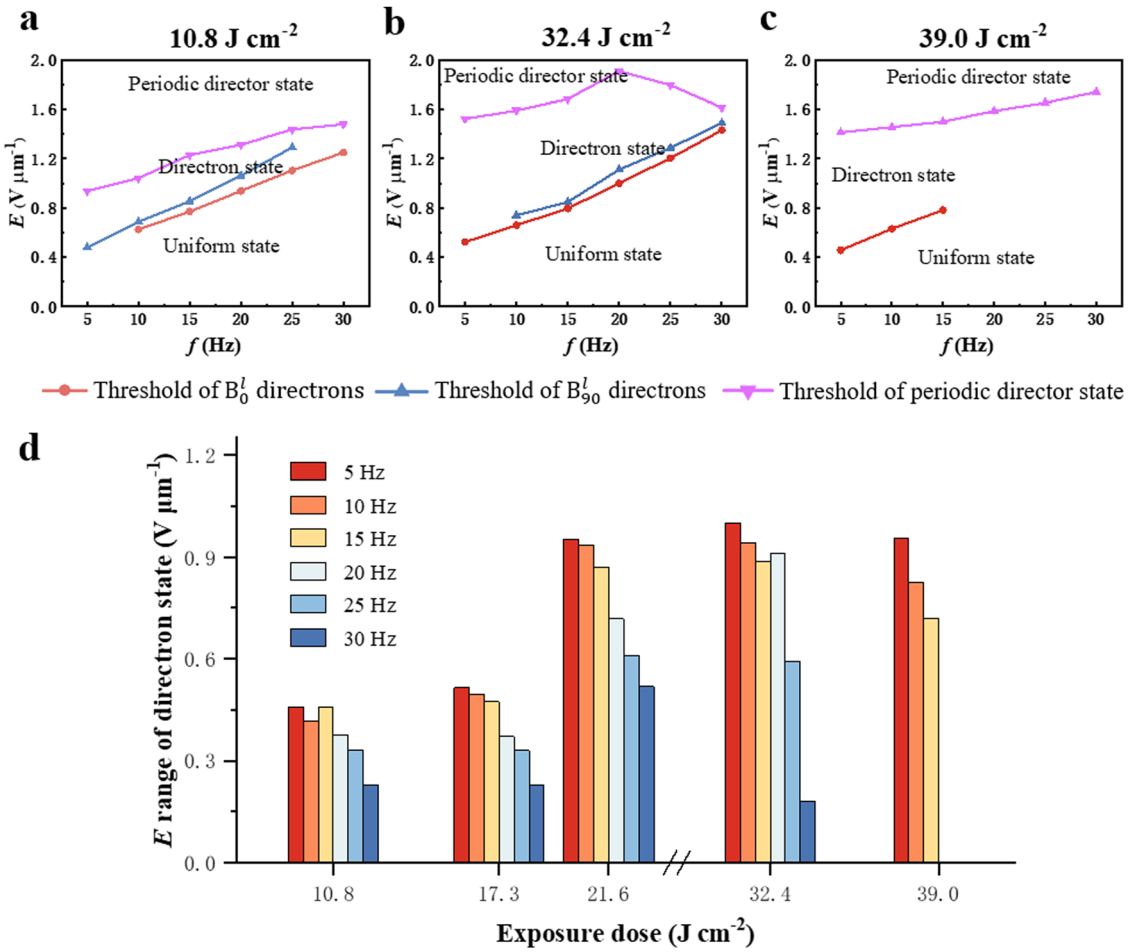

Fig. 2 E–f stability diagrams for exposure doses of (a) 10.8 J cm^{-2}, (b) 32.4 J cm^{-2}, and (c) 39 J cm^{-2}. Red, blue and purple lines represent the thresholds of B_0^l directrons, B_{90}^l directrons and the periodic director state, respectively. (d) E range histograms of directron state for different frequencies and exposure doses.

symmetry and directron width. The B_0^l and B_{90}^l directrons show mirror symmetry about two different planes, *i.e.*, the *xz* plane in Fig. 1b and the *yz* plane in Fig. 1c. The B_0^l directrons have almost the same width from head to tail, while the B_{90}^l directrons have a slightly larger width toward the tail. The length and width of B_0^l directrons are about 18 μm and 16 μm, and those of B_{90}^l directrons are about 20 μm and 24 μm.

Optimization of exposure dose for directron generation

The anchoring energy of the aligning layer plays an important role in directron generation, both for (+,+)-nematics aligned with photoalignment and for (−,−)-nematics aligned with surface chemistry in high-frequency electric field,[17,22] where the pair of signs denote the signs of dielectric and conductivity anisotropies. Directrons generated in materials and electric fields that are similar to our work, *i.e.*, (−,−)-nematics and low-frequency electric fields, involve azimuthal and polar oscillations of localized directors away from the initial alignment.[15] It is reasonable to speculate that the azimuthal and polar anchoring energies of the photoalignment layer are crucial to the formation of directrons. The anchoring energy of the SD1 layer, influenced by the photo-induced ordering, strongly depends on the exposure dose in photoalignment. It is necessary to examine the optimum exposure dose for directron generation.

The stability diagrams characterizing the dependence of the four states of director configurations, including directrons, on the electric field frequency and amplitude, for different exposure doses between 10.8 J cm^{-2} and 39.0 J cm^{-2} are shown in Fig. 2a–c and Fig. S3 (ESI†). As the electric field amplitude E increases above some frequency-dependent threshold E_0^l (red lines), B_0^l directrons first nucleate randomly from the uniform state and move in the cell. Once E exceeds another, larger threshold E_{90}^l (blue lines), B_0^l and B_{90}^l directrons coexist, while only B_{90}^l directrons remain for continuously increasing E. Finally, when E increases above certain even larger threshold E_{pd} (purple lines), the directron state is replaced by the periodic director state without another uniform state between them, dissimilar to the situation described for rubbing alignment. It is found that the effective range of E for directrons to stably exist are closely related to the exposure dose during the photoalignment process. Directrons form over relatively broad E ranges for the exposure doses of 21.6 J cm^{-2} and 32.4 J cm^{-2}. The E range of the directron state for different frequencies and exposure doses are displayed as histograms in Fig. 2d. For further quantitative comparison, this is defined as the difference between E_{pd} and E_0^l, or that between E_{pd} and E_{90}^l if no B_0^l directrons exist. For smaller exposure doses of 10.8 J cm^{-2} and 17.3 J cm^{-2}, the E ranges of the directron state are relatively narrow.

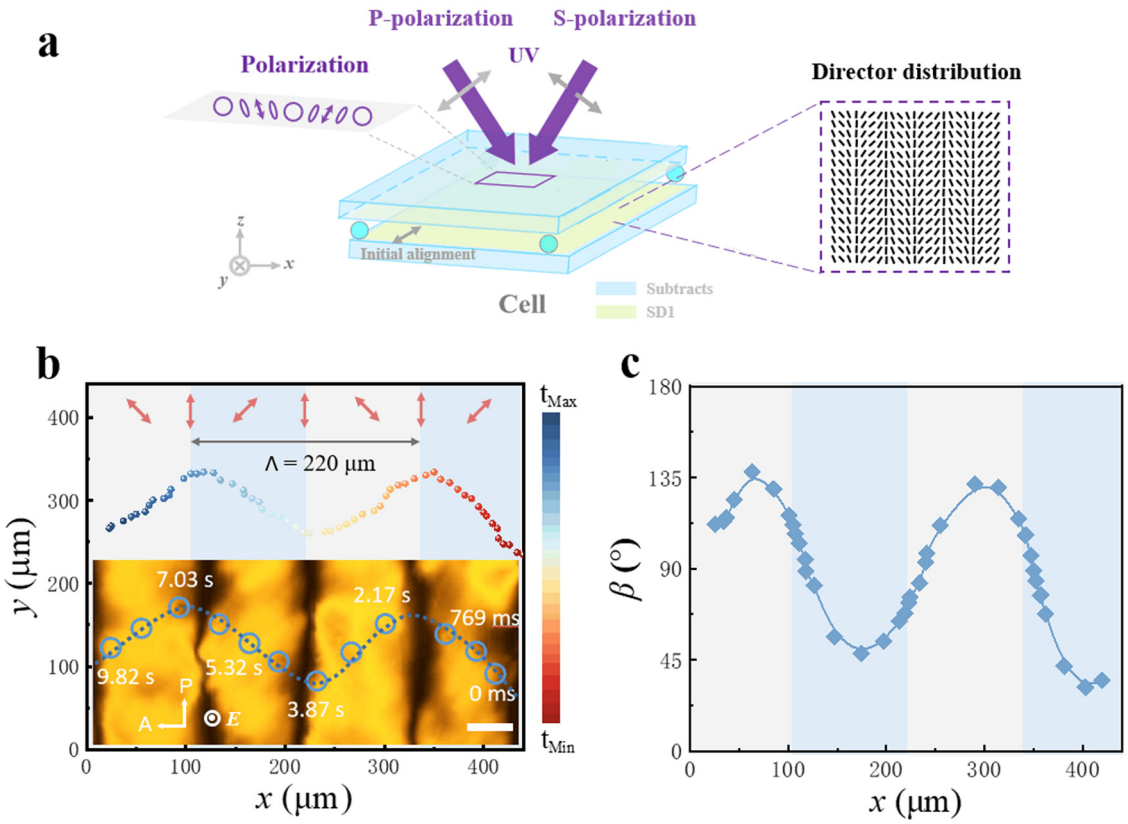

Fig. 3 Trajectory engineering of directrons *via* (a) polarization holography alignment technique with two OLP beams. (b) Zigzag trajectory of B_{90}^l directron with the alignment period of 220 μm and applied electric field of 1.21 V $μm^{-1}$. Red arrows indicate alignment directions. The inset shows the corresponding POM images of the directron at different time. ***E*** indicates the electric field perpendicular to the *xy* plane, A and P signify the analyzer and polarizer parallel to the *x* and *y* axis, respectively.The scale bar is 50 μm. (c) The angle between the motion directon of directron and the *y* axis.

When the exposure dose increases to 21.6 J cm^{-2}, the E range for the directron state is nearly doubled. The cell with a larger exposure dose of 32.4 J cm^{-2} has the largest E range of the directron state at most of the frequencies, which is selected as the optimum exposure dose in the following experiments. While the exposure dose reaches 39.0 J cm^{-2}, directrons are unable to appear at frequencies in the range of 20 Hz $\leq f \leq$ 30 Hz.

Zigzag directron trajectory

The multidomain photoalignment with high resolution by means of polarization holography is a feasible approach to design intricate periodic alignment fields for more complicated directron trajectories, and to evaluate the resolution of directron trajectory engineering simultaneously. For better multidomain alignment, the LC cell was photo-aligned homogeneously along the y axis in advance before being photo-aligned periodically by the polarization holography alignment technique,[28] with two coherent waves of orthogonal linear polarizations (OLPs) (Fig. 3a). In the optical interference field of the two incident beams, as illustrated in Fig. 3a, polarization ellipticities are modulated periodically and gradually between 0 and 1. Besides, polarization azimuths are $\pm\,\pi/4$ and vary by 90 degrees near each boundary point with a polarization ellipticity of 1. The initial uniform alignment was rewritten periodically by the elliptically polarized light in the interference field, owing to the photo-reorientation mechanism of SD1 molecules.[29,30] The alignment directions of azo dye photoalignment agents, induced by elliptically polarized light, vary with polarization ellipticities.[31] In detail, the eventual alignment directions gradually range from y axis to the minor axis of the elliptically polarization, as the polarization ellipticities decrease from 1 to 0 (Fig. 3b). The alignment field has alternate regions with gradually changing alignment directions symmetry about the y axis, resulting in alternate LC regions with splay elastic deformation (Fig. 3a).

The incident exposure dose is constant in polarization holography of small recording angles.[32] The effective torque model of azo dye photoalignment agents[31] implies that the effective exposure doses of elliptically polarized light decrease as the polarization ellipticities increase. In other words, the effective exposure doses in the resulting light field are inhomogeneous. The dependence of E_0^l and E_{90}^l, namely the electric field amplitude thresholds of B_0^l and B_{90}^l directrons, on the exposure dose of linearly polarized light is analyzed in Fig. S4 (ESI†). The thresholds at frequencies of 10 Hz, 15 Hz, and 20 Hz are less sensitive to exposure dose. Accordingly, the frequency of 20 Hz was employed in directron trajectory engineering with polarization holography. The zigzag trajectory of B_{90}^l directrons along the x axis, with the alignment period of 220 μm and at an applied electric field of 1.21 V μm^{-1}, is shown in Fig. 3b and Movie 1 (ESI†). The trajectory deflection with respect to the x axis, characterized by the angle between the central axis of trajectory and the x axis, is measured to be below 3 degrees. On the whole, the angle between the motion direction of directrons and the y axis, β, varies periodically from about 45 to 135 degrees as depicted in Fig. 3c. The B_{90}^l directrons roughly move perpendicularly to the alignment direction at each point of the periodic alignment field, similar to that with uniform alignment. These results demonstrate that the polarization holography alignment technique with two OLP beams is capable of steering directrons along zigzag trajectories.

It is noteworthy that polarization holography has spatially variant polarizations in each interference period, hence can supply high-resolution periodic photoalignment to evaluate the resolution of directron trajectory engineering at the same time. The resolution of directron trajectory engineering is defined as the minimum size of alignment domain required to maintain a segment of steerable directron trajectory. To determine the resolution that can be obtained by the polarization holography alignment technique with two OLP beams, the directron trajectories for different alignment periods were investigated. The alignment periods were varied by adjusting the incident angle between the two interference beams in the photoalignment process. The tested alignment periods are 60 μm, 113 μm, 160 μm, 220 μm, and 440 μm. The directron trajectories evolve from the irregular fluctuation mode into the periodic zigzag mode as the alignment periods increase (Fig. 4a and Movie S2, ESI†). In the fluctuation mode, with relatively small alignment periods of 60 μm and 113 μm, directrons basically move along the x axis with fluctuations of tens of micrometers (Fig. 4b). In the zigzag mode, diretrons propagate in a zigzag path steered by the predesigned periodic alignment configuration, with relatively large alignment periods of 160 μm, 220 μm, and 440 μm (Fig. 4b and Fig. S5, ESI†). The trajectory width w, *i.e.*, the displacement of directrons in the y direction, is approximately linear with the alignment period (Fig. 4a, red line). The ratio of trajectory width to alignment period increases in the fluctuation mode and becomes saturated in the zigzag mode (Fig. 4a, blue line). It can be concluded that the resolution of directron trajectory engineering by polarization holography of two OLP beams is in the range of 56 μm to 80 μm, nearly three to four times the directron length.

Fishhook-shaped directron trajectory

To explore another complex directron trajectory, the LC cell sample was also photo-aligned periodically by polarization holography alignment, with two coherent waves of orthogonal circular polarizations (OCPs) (Fig. 5a). The polarization

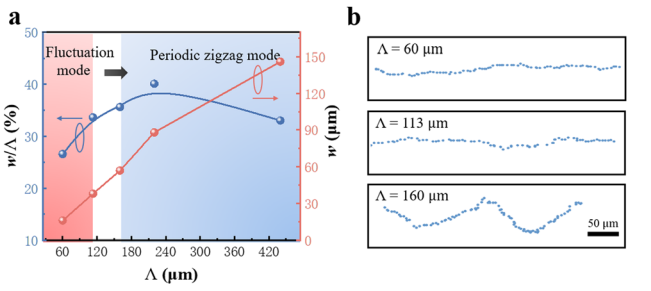

Fig. 4 Trajectory evolution of directrons with increasing alignment periods. (a) The ratio of trajectory width to alignment period (blue line), and the trajectory width (red line) for different alignment periods. (b) The trajectories of B_{90}^l directrons for alignment periods of 60 μm, 113 μm, and 160 μm. w and Λ are trajectory width and alignment period, respectively.

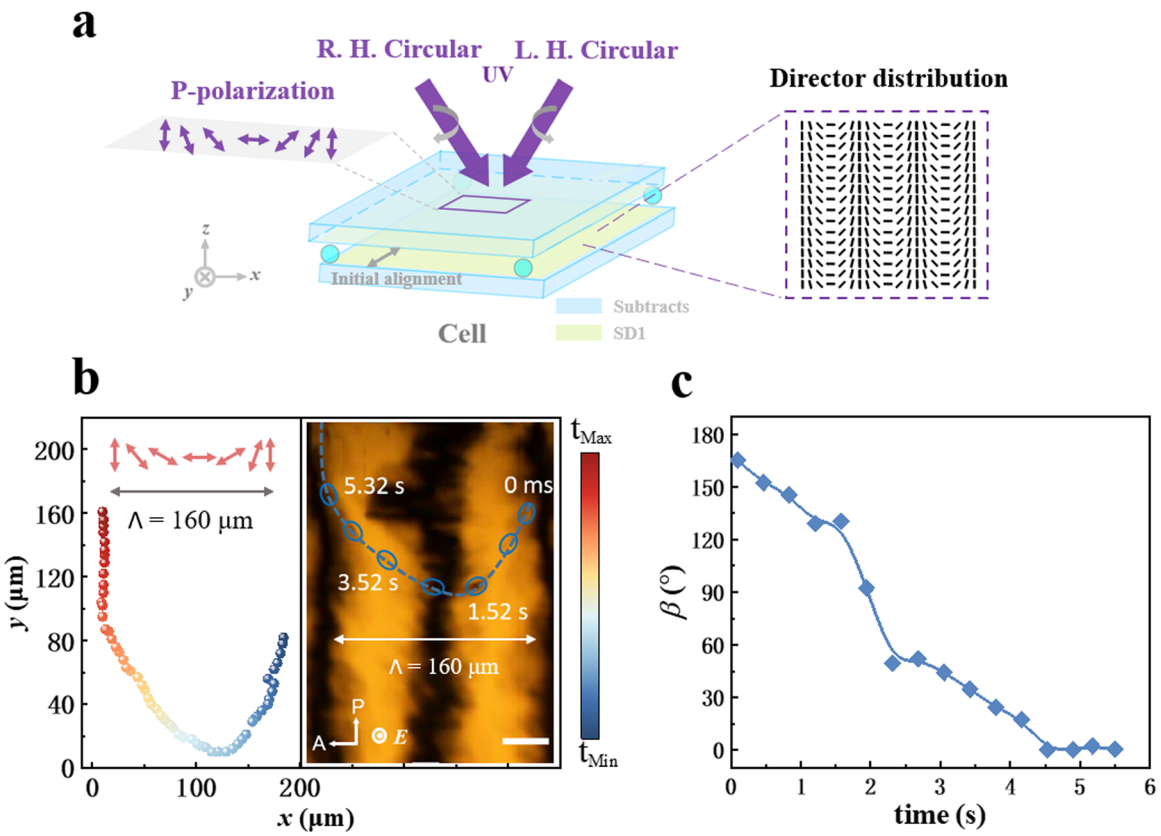

Fig. 5 Trajectory engineering of directrons *via* (a) polarization holography alignment technique with two OCP beams. (b) Fishhook-shaped trajectory of B_0^l directron with the alignment period of 160 μm in an electric field of 1.00 V μm^{-1}. Red arrows indicate alignment directions. The inset shows the corresponding POM images of the directron at different time. ***E*** indicates the electric field perpendicular to the *xy* plane, A and P signify the analyzer and polarizer parallel to the *x* and *y* axis, respectively. The scale bar is 50 μm. (c) The angle between the motion direction of directrons and the *y* axis.

azimuths were modulated periodically between ± π/2 in the optical interference field of the two incident beams, as illustrated in Fig. 5a. The resulting alignment directions gradually change from the *y* axis to the *x* axis in half an alignment period (Fig. 5b). As a result, the nematic LCs in the cell experience alternate regions with splay and bend elastic deformations, respectively (Fig. 5a). The fishhook-shaped trajectory of B_0^l directrons, with alignment period of 160 μm and an electric field of 1.00 V μm^{-1} applied, is shown in Fig. 5b and Movie S3 (ESI†). The angle between the motion direction of the directron and the *y* axis, *β*, varies continuously from almost 180 to 0 degrees as shown in Fig. 5c. The B_0^l directrons basically move parallel to the alignment direction at each point in the alignment period, similar to that with uniform alignment. It is therefore verified that the polarization holography alignment technique with two OCP beams can manipulate directrons along fishhook-shaped trajectories. In addition, no directrons were found to nucleate in the LC regions with bend elastic deformation. All directrons were generated from the LC regions with splay elastic deformation and then randomly turn left or right to the nearest neighboring LC region with the same elastic deformation.

Conclusions

In summary, we have demonstrated the feasibility of designing complex alignment layers *via* photoalignment to realize complicated trajectories of directrons. It is found that the generation of directrons is closely related to the exposure dose during the alignment process. The optimum exposure dose for directrons to form over a broad range of electric field amplitudes and frequencies is 32.4 J cm^{-2} for the alignment layers with 1 wt% SD1. On this basis, zigzag and fishhook-shaped trajectories of directrons are demonstrated by employing the polarization holography alignment technique with two OLP beams and two OCP beams, respectively. The resolution for zigzag manipulation of directrons is in the range of 56 μm to 80 μm, nearly three to four times the length of directrons. Our work promotes the variety of possible applications of directrons by enriching their forms of motion. We envisage future studies in which directrons are steered along zigzag trajectories to enhance reaction efficiency in chemical systems, and along fishhook-shaped trajectories to transport microcargoes into multiple directional channels with equal spacing. More intricate nonperiodic directron trajectories are expected to be achieved by making use of functional photomanipulatable LCs,[33–35] or by adopting more advanced photoalignment techniques such as digital micromirror photopatterning[36] and plasmonic projection photoalignment.[37,38]

Author contributions

Conceived the project and co-supervised the research: L.-J C. and S.-S L. Performed the experimental studies: K.-H W.

Analyzed the data: L.-J C., S.-S L., and K.-H W. Contributed through discussions and writing the manuscript: L.-J C., S.-S L., K. -H W., I. D., and Y. S.

Conflicts of interest

The authors declare no competing interests.

Acknowledgements

This work was supported by the National Natural Science Foundation of China (NSFC) (No. 62175206, 62075186); National Key R&D Program of China (No. 2022YFA1203700, No. 2019YFA0905800). The authors would like to acknowledge Hao Wang for helping with measuring dielectric constants and conductivities.

Notes and references

1 L. Lam and J. Prost, *Solitons in liquid crystals*, Springer, New York, 1992.
2 P. S. Marcus, Jupiter's Great Red Spot and Other Vortices, *Annu. Rev. Astron. Astrophys.*, 1993, **31**, 523–569.
3 J. Sommeria, S. D. Meyers and H. L. Swinney, Laboratory simulation of Jupiter's Great Red Spot, *Nature*, 1988, **331**, 689–693.
4 M. W. Ray, E. Ruokokoski, S. Kandel, M. Möttönen and D. S. Hall, Observation of Dirac monopoles in a synthetic magnetic field, *Nature*, 2014, **505**, 657–660.
5 A. N. Bogdanov and C. Panagopoulos, Physical foundations and basic properties of magnetic skyrmions, *Nat. Rev. Phys.*, 2020, **2**, 492–498.
6 W. Helfrich, Alignment-Inversion Walls in Nematic Liquid Crystals in the Presence of a Magnetic Field, *Phys. Rev. Lett.*, 1968, **22**, 1342.
7 I. I. Smalyukh, Knots and other new topological effects in liquid crystals and colloids, *Rep. Prog. Phys.*, 2020, **83**, 106601.
8 I. I. Smalyukh, Y. Lansac, N. A. Clark and R. P. Trivedi, Three-dimensional structure and multistable optical switching of triple-twisted particle-like excitations in anisotropic fluids, *Nat. Mater.*, 2010, **9**, 139–145.
9 P. J. Ackerman and I. I. Smalyukh, Diversity of knot solitons in liquid crystals manifested by linking of preimages in torons and hopfions, *Phys. Rev. X*, 2017, **7**, 011006.
10 M. Peccianti, C. Conti, G. Assanto, A. De Luca and C. Umeton, Routing of anisotropic spatial solitons and modulational instability in liquid crystals, *Nature*, 2004, **432**, 733–737.
11 G. Assanto *Nematicons: spatial optical solitons in nematic liquid crystals*, John Wiley & Sons, New Jersey, Vol. 74, 2012.
12 M. Peccianti, C. Conti, G. Assanto, A. De Luca and C. Umeton, All-optical switching and logic gating with spatial solitons in liquid crystals, *Appl. Phys. Lett.*, 2002, **81**, 3335–3337.
13 S. Perumbilavil, A. Piccardi, R. Barboza, O. Buchnev, M. Kauranen, G. Strangi and G. Assanto, Beaming random lasers with soliton control, *Nat. Commun.*, 2018, **9**, 1–7.
14 B.-X. Li, V. Borshch, R.-L. Xiao, S. Paladugu, T. Turiv, S. V. Shiyanovskii and O. D. Lavrentovich, Electrically driven three-dimensional solitary waves as director bullets in nematic liquid crystals, *Nat. Commun.*, 2018, **9**, 2912.
15 B.-X. Li, R.-L. Xiao, S. Paladugu, S. V. Shiyanovskii and O. D. Lavrentovich, Three-dimensional solitary waves with electrically tunable direction of propagation in nematics, *Nat. Commun.*, 2019, **10**, 3749.
16 S. Aya and F. Araoka, Kinetics of motile solitons in nematic liquid crystals, *Nat. Commun.*, 2020, **11**, 3248.
17 Y. Shen and I. Dierking, Dynamic dissipative solitons in nematics with positive anisotropies, *Soft Matter*, 2020, **16**, 5325–5333.
18 H. R. Brand, C. Fradin, P. Finn, W. Pesch and P. Cladis, Electroconvection in nematic liquid crystals: comparison between experimental results and the hydrodynamic model, *Phys. Lett. A*, 1997, **235**, 508–514.
19 O. D. Lavrentovich, Design of nematic liquid crystals to control microscale dynamics, *Liq. Cryst. Rev.*, 2020, **8**, 59–129.
20 Y. Shen and I. Dierking, Dynamics of electrically driven solitons in nematic and cholesteric liquid crystals, *Commun. Phys.*, 2020, **3**, 1–9.
21 Y. Shen and I. Dierking, Electrically tunable collective motion of dissipative solitons in chiral nematic films, *Nat. Commun.*, 2022, **13**, 1–12.
22 S. Das, S. Roh, N. Atzin, A. Mozaffari, X. Tang, J. J. de Pablo and N. L. Abbott, Programming Solitons in Liquid Crystals Using Surface Chemistry, *Langmuir*, 2022, **38**, 3575–3584.
23 Y. Shen and I. Dierking, Recent progresses on experimental investigations of topological and dissipative solitons in liquid crystals, *Crystals*, 2022, **12**, 94.
24 B.-X. Li, R.-L. Xiao, S. V. Shiyanovskii and O. D. Lavrentovich, Soliton-induced liquid crystal enabled electrophoresis, *Phys. Rev. Res.*, 2020, **2**, 013178.
25 R. Zhang, A. Mozaffari and J. J. de Pablo, Autonomous materials systems from active liquid crystals, *Nat. Rev. Mater.*, 2021, **6**, 437–453.
26 L.-L. Ma, S.-S. Li, W.-S. Li, W. Ji, B. Luo, Z.-G. Zheng, Z.-P. Cai, V. Chigrinov, Y.-Q. Lu, W. Hu and L.-J. Chen, Rationally Designed Dynamic Superstructures Enabled by Photoaligning Cholesteric Liquid Crystals, *Adv. Opt. Mater.*, 2015, **3**, 1691–1696.
27 V. Chigrinov, H. S. Kwok, H. Takada and H. Takatsu, Photo-aligning by azo-dyes: physics and applications, *Liq. Cryst. Tod.*, 2005, **14**, 1–15.
28 S. S. Li, Y. Shen, Z. N. Chang, W. S. Li, Y. C. Xu, X. Y. Fan and L. J. Chen, Dynamic cholesteric liquid crystal superstructures photoaligned by one-step polarization holography, *Appl. Phys. Lett.*, 2017, **111**, 231109.
29 A. K. Srivastava, X. Wang, S. Gong, D. Shen, Y. Q. Lu, V. G. Chigrinov and H. S. Kwok, Micro-patterned photo-aligned ferroelectric liquid crystal Fresnel zone lens, *Opt. Lett.*, 2015, **40**, 1643–1646.

30 E. A. Shteyner, A. K. Srivastava, V. G. Chigrinov, H.-S. Kwok and A. D. Afanasyev, Submicron-scale liquid crystal photo-alignment, *Soft Matter*, 2013, **9**, 5160–5165.
31 A. Y.-G. Fuh, Y.-D. Chen, C.-K. Liu and K.-T. Cheng, Azo dye adsorption effect induced by elliptically polarized light in azo dye-doped liquid crystals, *Dyes Pigm.*, 2012, **92**, 949–953.
32 L. Nikolova and T. Todorov, Diffraction efficiency and selectivity of polarization holographic recording, *Opt. Acta. Int. J. Opt.*, 1984, **31**, 579–588.
33 H. K. Bisoyi and Q. Li, Light-driven liquid crystalline materials: from photo-induced phase transitions and property modulations to applications, *Chem. Rev.*, 2016, **116**, 15089–15166.
34 R. S. Zola, H. K. Bisoyi, H. Wang, A. M. Urbas, T. J. Bunning and Q. Li, Dynamic control of light direction enabled by stimuli-responsive liquid crystal gratings, *Adv. Mat.*, 2019, **31**, 1806172.
35 H. K. Bisoyi and Q. Li, Liquid crystals: versatile self-organized smart soft materials, *Chem. Rev.*, 2021, **122**, 4887–4926.
36 P. Chen, B. Y. Wei, W. Hu and Y. Q. Lu, Liquid-crystal-mediated geometric phase: from transmissive to broadband reflective planar optics, *Adv. Mater.*, 2020, **32**, 1903665.
37 Y. Guo, M. Jiang, C. Peng, K. Sun, O. Yaroshchuk, O. Lavrentovich and Q. H. Wei, High-resolution and high-throughput plasmonic photopatterning of complex molecular orientations in liquid crystals, *Adv. Mater.*, 2016, **28**, 2353–2358.
38 M. Jiang, Y. Guo, H. Yu, Z. Zhou, T. Turiv, O. D. Lavrentovich and Q. H. Wei, Low f-Number Diffraction-Limited Pancharatnam-Berry Microlenses Enabled by Plasmonic Photopatterning of Liquid Crystal Polymers, *Adv. Mater.*, 2019, **31**, 1808028.

